*Cardiovascular Engineering and Technology*, Vol. 10, No. 2, June 2019 *(© 2019)* pp. 225–241
https://doi.org/10.1007/s13239-019-00412-7

# Image-Based Flow Simulations of Pre- and Post-left Atrial Appendage Closure in the Left Atrium

DONGJIE JIA,[1] BYUNGHWAN JEON,[2,3] HYUNG-BOK PARK,[3,4] HYUK-JAE CHANG,[3,5] and LUCY T. ZHANG [1]

[1]Department of Mechanical, Aerospace & Nuclear Engineering, Rensselaer Polytechnic Institute, Troy, NY 12180, USA; [2]Brain Korea 21 PLUS Project for Medical Science, Yonsei University, Seoul, South Korea; [3]Yonsei-Cedars Sinai Integrative Cardiovascular Imaging Research Center, Yonsei University Health System, Seoul, South Korea; [4]Division of Cardiology, Department of Internal Medicine, International St. Mary's Hospital, Catholic Kwandong University College of Medicine, Incheon, South Korea; and [5]Division of Cardiology, Severance Cardiovascular Hospital, Yonsei University Health System, Seoul, South Korea

*(Received 6 November 2018; accepted 28 March 2019; published online 5 April 2019)*

Associate Editor Ajit P. Yoganathan oversaw the review of this article.

**Abstract**

*Purpose*—For patients with atrial fibrillation, the left atrial appendage (LAA) is often the site of thrombus formation due to low atrial ejection fraction that triggers strokes and other thromboembolic events. Recently introduced percutaneous LAA occlusion procedure is known to reduce LAA-induced strokes. Despite having the procedure, there are still 11% of the patients who continue to suffer from future strokes or transient ischemic attacks, not accounting for the procedural related complications. The high failure rate is largely due to the variabilities in LAA's shape, size, and contractility which may result in ineffectiveness of this procedure. To correctly identify the candidates and evaluate the effectiveness of the procedure, we rely on patient-specific CT scans which provides the exact LA and LAA geometries and predictive hemodynamic analysis to assist in evaluating quantitative flow parameters pre- and post-LAA occlusion procedures. Hemodynamic parameters are critical to predict adverse hemodynamic flow patterns in LAA as well as the effectiveness of LAA closure in individual patient. The aim of this paper is to establish an image-based patient-specific computational fluid dynamic (CFD) simulation framework specific to the prediction of treatment outcomes of LAA closure with atrial fibrillation. This framework utilizes automated LA/LAA image segmentation which yields significant reduction in image processing. One set of patient data with successful procedure outcome is used to illustrate the potential of the proposed framework.

*Methods*—The proposed LAA occlusion simulation framework is composed of several components: (1) a novel image segmentation procedure, which is fully-automated to identify LA/LAA geometries from CT images, (2) a finite-element mesh generation procedure which transforms the surface geometry into a 3-D volume mesh and properly identified boundary planes, (3) performing CFD simulations with atrial fibrillation flow boundary conditions, and (4) analyzing flow characteristics (velocity, flow patterns, streamlines, vortices) within the LA for before and after LAA closure.

*Results*—Based on the LA/LAA segmentation of a 65 year old female patient with chronic atrial fibrillation, a CFD analysis was pursued to examine flow characteristics upon LAA closure. The results showed that the flow velocity magnitudes were significantly reduced by a maximum factor of 2.21, flow streamlines were greatly stabilized, and mitral outflow appeared to be more organized. Vortices were dramatically reduced in size, number, intensity, as well as duration. During diastole, the peak vortex diameter was reduced from 2.8 to 1.5 cm, while the vortex duration was reduced from 0.210 to 0.135 s. These flow characteristics all indicated a reduced risk in future thrombus formation and strokes based on the established relationship between flow and thrombus formation. For the patient case under study, the effectiveness of the procedure is predicted and found to be consistent with the actual procedural outcome.

*Conclusions*—This framework successfully predicted patient-specific outcome of a LAA closure procedure for one patient with atrial fibrillation. It can be further developed into a useful tool for pre-procedural planning and candidate selection. More patient data are necessary for further validation studies.

**Keywords**—Left atrial appendage, Computational fluid dynamics, Atrial fibrillation.

## INTRODUCTION

The left atrial appendage (LAA) is a long, tubular, hooked structure derived from the left atrium (LA).[40] This structure originally functions as a decompression chamber when the left atrial pressure is elevated.[40]

Address correspondence to Lucy T. Zhang, Department of Mechanical, Aerospace & Nuclear Engineering, Rensselaer Polytechnic Institute, Troy, NY 12180, USA. Electronic mail: zhanglucy@rpi.edu

Dongjie Jia and Byunghwan Jeon contributed equally in this work.

However, in pathologic conditions such as atrial fibrillation, enlarged and fibrillating LA and LAA serve as sources of thrombus formation thus causing strokes and other thromboembolic events.[40,40,49] Most dramatically, up to 90% of embolic strokes are originated from dilated, motionless pouch-like LAAs.[9,22] Furthermore, in a recent study, LAA was shown to trigger atrial fibrillation, appearing to be responsible for arrhythmia in 27% of the patients.[8]

Recently, percutaneous LAA occlusion procedures were introduced to reduce stroke risk.[37,41] This percutaneous procedure is to introduce device delivery catheter and establish LAA occlusion device without surgical opening of the chest. The catheter enters from femoral vein puncture site through inferior vena cava and interatrial septum, finally approaching LAA ostium. Percutaneous LAA occlusion is an evolving therapy, which had been taken into consideration for patients with atrial fibrillation with a high stroke risk and contraindications for oral anticoagulants. Even though all patients with increased stroke risk and contraindications to oral anticoagulants are possible candidates for LAA closure, there are still 11% of the patients with successful LAA closure suffer strokes or transient ischemic attacks, not accounting for procedure-related complications. The reason for such a high failure rate is mostly due to further thrombosis formation in the LA upon LAA closure.[22] In a recent review on percutaneous LAA occlusion study,[6] the authors emphasized the importance of proper patient selection.

The amount of thrombus formation inside LAA varies greatly among individuals due to its variabilities in its shape (morphology), volume size, and contractile function.[15,51] LAA is generally classified into four types by morphology: chicken-wing (18.3%), windsock (46.7%), cauliflower (29.1%), and cactus (5.9%).[51] Based on a recent study,[27] the volume size of LAA also varies greatly by morphology, typically ranges in$12.6 \pm 5.2$ ml. The contractile function (or dysfunction) of LAA is related to thromboembolic complications, quantified by means of computing LAA ejection fraction (EF) using maximum and minimum LAA areas, and is found to be in the range of $39 \pm 8\%$.[44] Collectively, these variabilities have strong effects on the blood flow characteristics inside LA and LAA.[15,17]

It is known that hemodynamics, such as velocity, flow pattern, vortices significantly affect the process of thrombus formation in LA and LAA.[16–17,40,49] However, in clinical practice, besides the LAA emptying velocity obtained from transesophageal echocardiography (TEE),[17] other hemodynamic parameters, particularly in the thrombus regions, cannot be assessed accurately using TEE, as it can either falsely label muscles as thrombi or miss identifying thrombi hidden in one of the lobes.[7] Therefore, a better approach needs to be sought out. Since the presence of thrombus is critical in identifying the LAA closure procedure candidates, studying individual cases in an effective and efficient manner allows us to gain better prediction on future thrombus formation. The first logical step is then to predict and evaluate the efficacy of performing such a procedure using non-invasive means. From this perspective, computational fluid dynamic (CFD) simulation of velocity, flow pattern, and vortices in LA and LAA can therefore provide useful information for the prediction of LAA thrombus formation, which can then be used with or in place of clinical TEE to drastically increase the accuracy in identifying the right candidates. Moreover, computer simulation can also be used to predict the necessity and the efficacy of a LAA occlusion procedure.

Prior CFD studies have been done to analyze the hemodynamics in different LAA morphologies to identify potential relationships between the morphology and the risk of thrombotic events.[10,18] Their simulation studies showed that LAA with a specific morphology such as cauliflower results in higher risk of thrombosis. Otani *et al.* proposed a CFD framework for hemodynamic analysis and its feasibility in understanding the mechanism of intracardiac thrombosis and stroke in individual patients with LA structural remodeling.[38] Masci *et al.* used a CFD model to quantify the hemodynamic implications of atrial fibrillation on a patient-specific basis.[32] All the studies have a similar goal which is to identify the relationship between thrombosis and patient-specific LA model through hemodynamic analysis. Several prior attempts have also been made to perform hemodynamic evaluations[33,35,53] in predictive medicine using patient-specific data. In Mittal *et al.*'s work,[35] the authors reviewed the current status of the emerging trends and challenges in cardiovascular modeling and simulations. It emphasized the clear need to create an efficient and automated pipeline for generating CFD-ready geometry from medical images. Automatic 3D segmentation without any operators' manual interaction is crucial and is one of the challenges for clinically applicable CFD simulations. As of today, no studies are focused on the hemodynamic changes in the LA pre- and post-LAA occlusion.

In this study, we intend to address the gap by proposing a CFD framework using patient-specific image to evaluate the potential effectiveness of percutaneous LAA occlusion procedure. Our study, therefore, is aimed to establish a simulation tool for predicting patient-specific treatment outcomes of LAA closures in severely diseased atrial fibrillation patients. There are two major contributions in this work: (1) we propose a fully-automated LA/LAA segmentation

approach, and (2) we propose a computational framework in assessing hemodynamic changes of a LAA occlusion procedure using patient-specific CT images. This framework provides the basis in developing a critical clinical assessment tool for percutaneous LAA occlusion procedures. Even though imaged-based CFD analysis has been proposed for many clinical applications, it is the first time such a framework is proposed in the context of LAA occlusion procedures.

The rest of the paper is organized as follows: in "Materials and Methods" section, we provide the workflow for an automated LA/LAA segmentation, meshing, and CFD analysis based on a patient-specific case. In "Results" section, the CFD results are presented. In "Discussion" section, we discuss the hemodynamic findings of the study. Finally, study limitations are presented in "Study Limitations" section and the conclusions are drawn in "Conclusions" section.

## MATERIALS AND METHODS

### *Patient-Specific LA/LAA Simulation Workflow*

The goal of this study is to establish a simulation framework that uses CFD analysis to predict patient-specific percutaneous LAA closure. The framework is targeted for patients with atrial fibrillation. Using patient-specific computed tomography angiography (CT) scans, hemodynamic analysis for pre- and post-LAA closure are performed and then compared. The work flow of the framework is described in Fig. 1. It includes two major components: (1) automated imaging processing using patient-specific CT scans and (2) CFD simulation using the processed image data. The details are as follows:

(1) Retrieve CT images from a patient. Use our fully-automated image segmentation technique to register, and accurately and efficiently identify LA and LAA from CT images;
(2) Process segmented image into CAD formats for pre- and post-LAA occlusion geometries;
(3) Setup simulation model that includes volume discretization using finite elements, defining inflow (pulmonary arteries) and outflow (mitral valve) boundaries, and applying atrial fibrillation inflow and outflow boundary conditions;
(4) Perform CFD flow simulation until flow reaches periodicity over each cardiac cycle;
(5) Analyze flow characteristics, e.g. velocity, pressure, streamline, vortices, in LA and LAA, and compare them for pre- and post-LAA occlusion;
(6) Determine the suitability of the patient for percutaneous LAA closure based on the changes in flow characteristics.

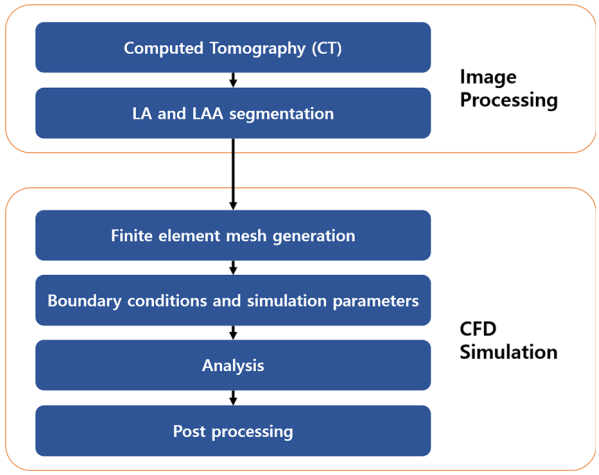


**FIGURE 1. Work flow of the simulation framework.**

In this study, we use CT images of a patient who has permanent atrial fibrillation as a pilot study. The candidate is a 67 year-old female who has chronic atrial fibrillation. The patient has a LA with chicken-wing type LAA. The LAA occlusion procedure for the candidate is successfully completed. The Institutional Review Board approved this study and waived the requirement for informed patient consent due to its retrospective nature.

### *Image Processing of LA and LAA*

The goal of image processing is to convert CT images into a 3D mesh ready for CFD simulations. Image segmentation tools such as Mimics and 3D-Doctor[1,34] typically offer semi-automatic segmentation. Depending on the operator's expertise, a successfully segmented LA and LAA usually takes 5–10 min per case. Localization is a prerequisite process that needs to be completed prior to the automated segmentation process. Manual placement of a central point of the LA in 3D volume is a time consuming process. In this work, we introduce a fully-automated technique that acquires and processes the patient-specific LA region from CT images within 0.5–1 min processing time. A fully-automated segmentation process is important as a higher throughput of studies can be performed and in the meantime avoids interactions with un-experienced operators. Such a fully-automated approach is able to consistently detect a central point inside LA using anatomic knowledge.

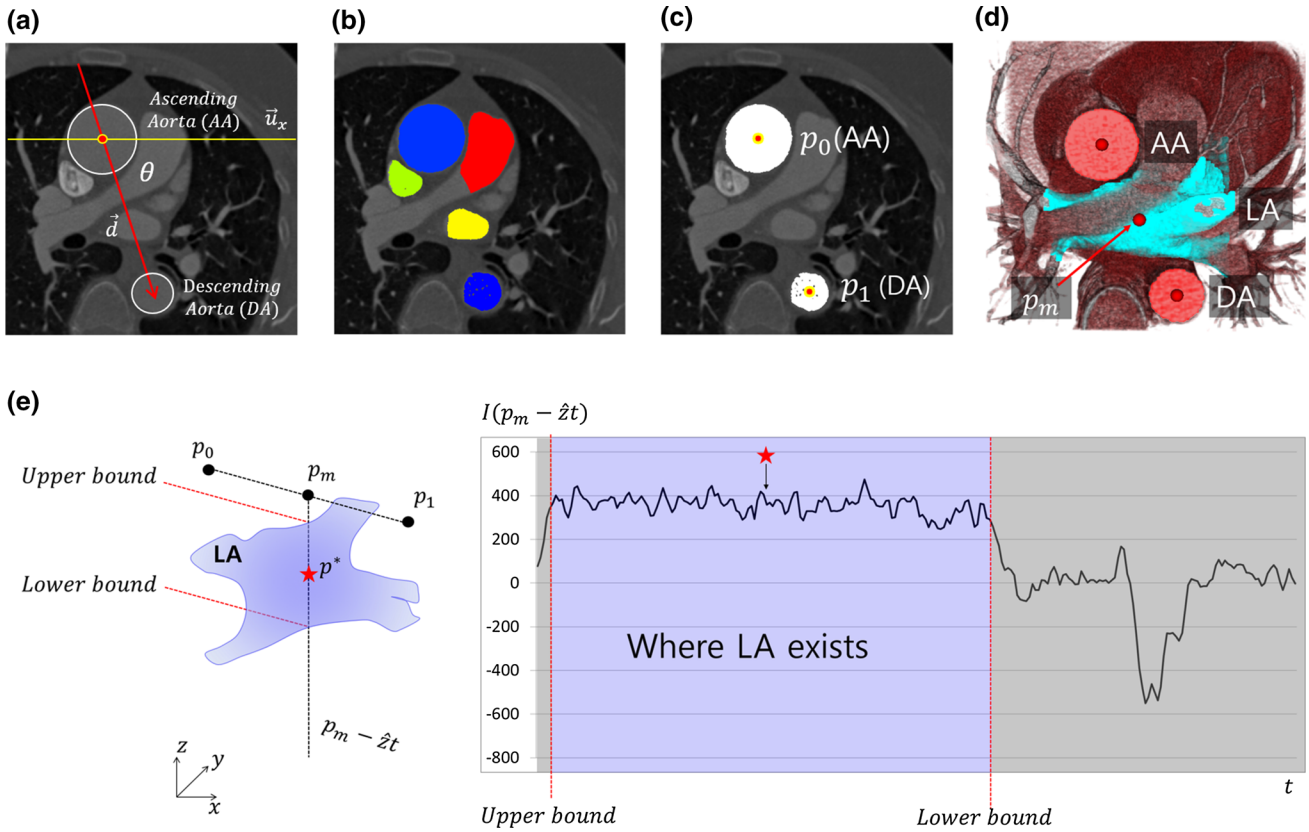


**FIGURE 2. LA seed detection process: (a) original image, (b) candidates for two aortas (AA and DA), (c) detected regions and their centroid points ($p_0$ and $p_1$), (d) all the results (AA, DA, LA) are visualized. LA region is anatomically located between them, (e) the profile of intensity responses along z-ray ($p_m - \vec{z}t$) is analyzed for detecting final 3D position $p^*$.**

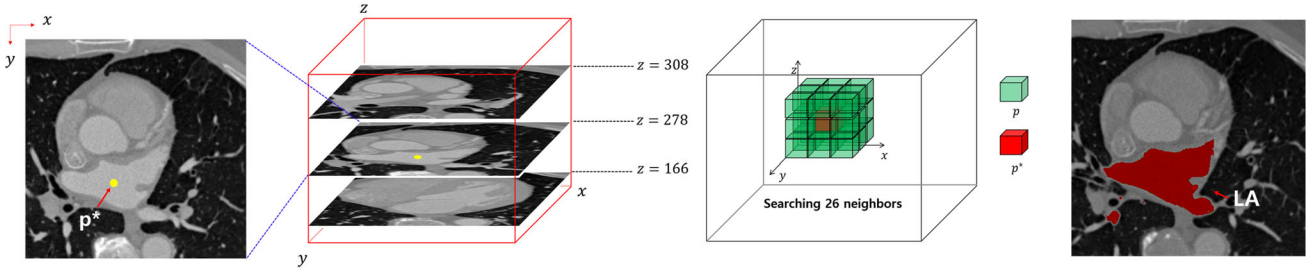


**FIGURE 3. Segmentation based on initial seed $p^*$: the region growing method requires an initial 3D point inside the LA, and the point can be detected automatically by using the method described in "Automatic LA Seed Point Detection" section. From the point, LA region is automatically found by Algorithm 1.**

In here, the LA region is segmented using a seed point in LA that is automatically detected from identified ascending and descending aortas. In this study, CT images ($I$) are reconstructed as $512 \times 512$ pixels with a pixel size of 0.38 mm $\times$ 0.38 mm. They are mapped using the Hounsfield unit (HU) with a value ranges between $-1000$ to 3000 HU, according to the constituent of the patient's body.

### *Automatic LA Seed Point Detection*

To automatically detect the LA seed point, we utilize the anatomical fact that LA is located between the ascending aorta (AA) and the descending aorta (DA) in an axial view, as shown in Fig. 2. The following steps are taken:

(1) Identify ascending aorta (AA) and descending aorta (DA) by detecting them in the axial view. Two aortas are simultaneously identified

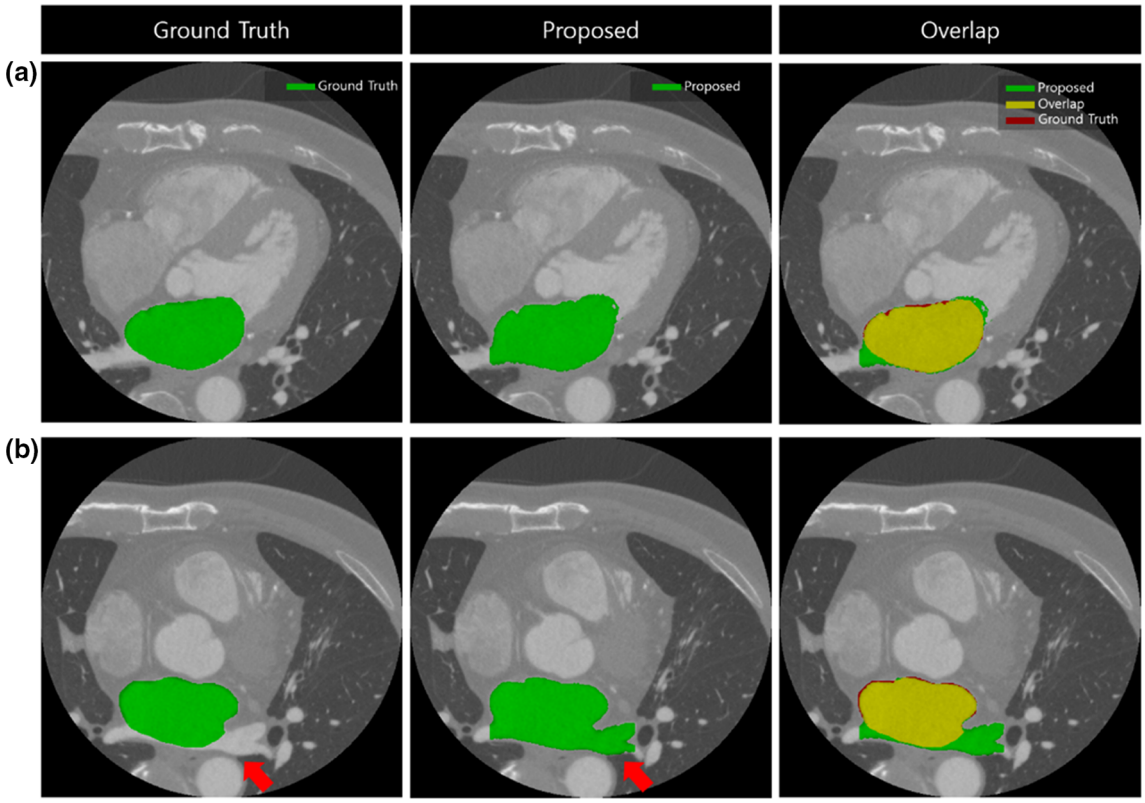


**FIGURE 4. Validation of the proposed segmentation method by comparing to the ground truth (GT) on different slices: (a) at $z = 155$. (b) at $z = 185$. The overlap regions between the GT and our segmented results are also identified. At the LA region, the two boundaries, GT and the result are almost overlapped. The only ''error'' is due to the difference of with or without PV. The proposed algorithm is designed to include some PV regions for simulations, as they are important parts to identify the inlets of the blood stream.**

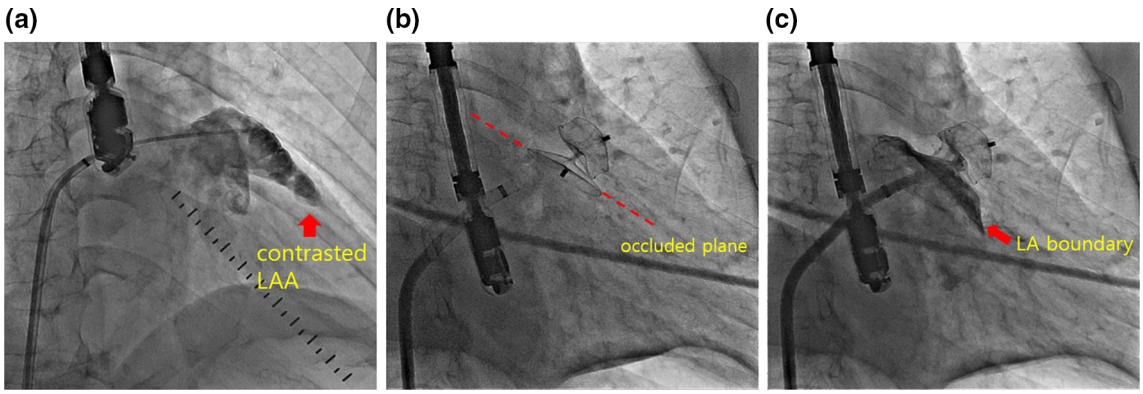


**FIGURE 5. X-ray images during the occlusion procedure of the current patient. (a) during contrast injection before the LAA procedure, (b) the well-deployed Amplatzer device after LAA procedure, (c) during contrast injection after LAA procedure.**

using their geometric anatomic relations such as the angle and the distance between AA and DA using the identification method detailed in Ref. 21 (Fig. 2a).

(2) Based on step 1, several 2D discrete candidates (Fig. 2b) are identified. AA and DA are then simultaneously detected from the candidates, labeled as $p_0$ and $p_1$ in Fig. 2c.

(3) From the two detected aortas, the centroid of the LA region is then identified and used as a seed point (Fig. 2d). The intensity response along $z$-axis domain $p_m - \vec{z}t$ is profiled from their mean point $p_m = (p_0 + p_1)/2$. The seed

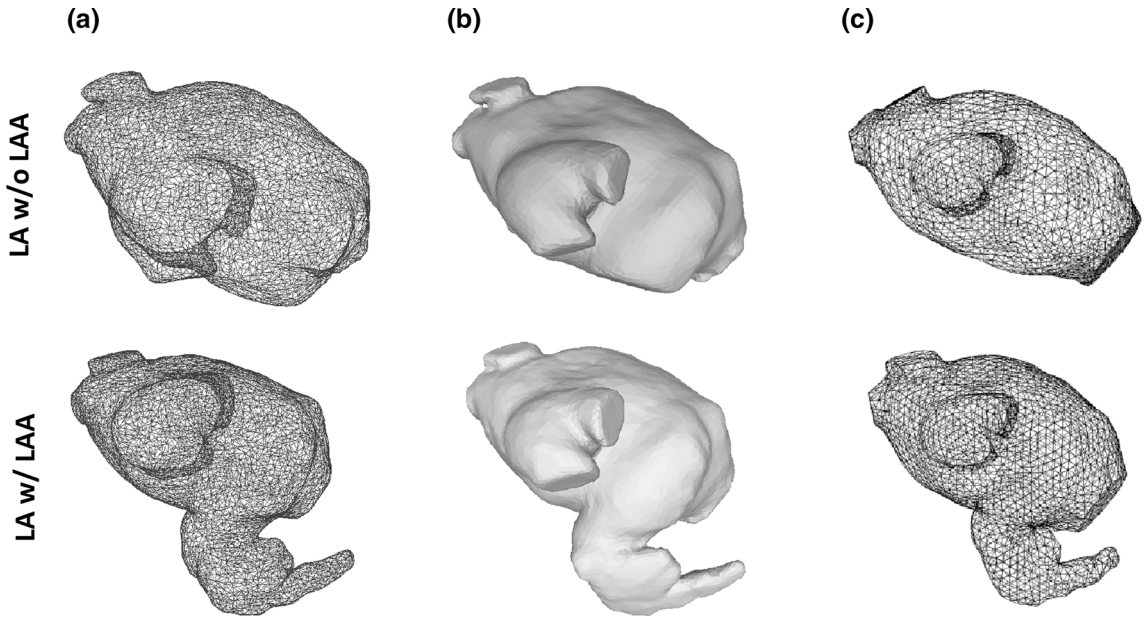


**FIGURE 6. 3D mesh construction process for LA with LAA (top) and without LAA (bottom): (a) surface meshing, (b) 3D part generation, and (c) volumetric meshing (opaque).**

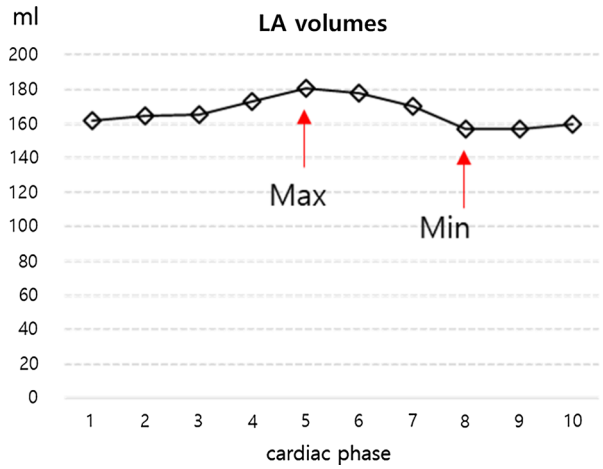


**FIGURE 7. Volume measurements of the left atrium with LAA over a cardiac cycle.**

point $p^*$ is finally detected in the middle of the plateau as $p_z^* = (\text{Upper bound}) + (\text{Lower bound})$, which is visually described in Fig. 2e. The area of plateau is identified by the error $|\mu_{AA} - I(p_m - \vec{z}t)| < \epsilon$ where $\mu_{AA}$ is an average HU value from the samples inside AA, and $\epsilon = 60\text{HU}$.

### *LA/LAA Segmentation*

Once the seed point in the LA is clearly detected, the segmentation can be achieved using a Bayesian inference region growing method that restricts growing volume based on the seed point. The segmentation algorithm is described in Algorithm 1, where the Bayesian's approach is used considering the intensity and the distance constraints derived from Ref. 3. In Algorithm 1, the input parameters $\mu_c$ and $\sigma_c$ are the expectation HU for LA contrast and its deviation, respectively. $p^*$ is the seed point inside LA described in Fig. 2; and $\delta_0$ and $l_0$ are the prior distance and threshold for the posterior probability, respectively. For local variables, $V$ is simply a 3D visit map which has dimensions equal to the original image $I$ and is mapped to 0 or 1 for visiting check. A queue $Q$ has a list of potential points to examine their neighboring points in 26 directional traveler considering 3D structures, which is illustrated in Fig. 3. $C = \{p_i | 1 \le i \le N = |C|\}$ is simply a point set which has 3D points finally forming the LA region.

This method is performed to expand the region from a seed point $p^*$ to a set of points $C$ with similar properties and then measure the intensity by posterior probability $P(A \mid I)$ using Bayes' inference, Eq. (1), until a geodesic distance criteria $\delta_0$ is satisfied. The final set $C$ which is the region of the LA is finally determined. The posterior $P(A \mid I)$ is derived from Bayes' inference:

$$\begin{aligned} P(A \mid I) &= P(I \mid A)P(A)/P(I) \\ &\propto P(I \mid A)P(A) \end{aligned} \tag{1}$$

where $I$ is a CT image and $A$ is a target object, respectively. The likelihood $P(I \mid A)$ is modeled for contrast HU and the prior $P(A)$ is set to be the LA region's prior distributions using the distance between

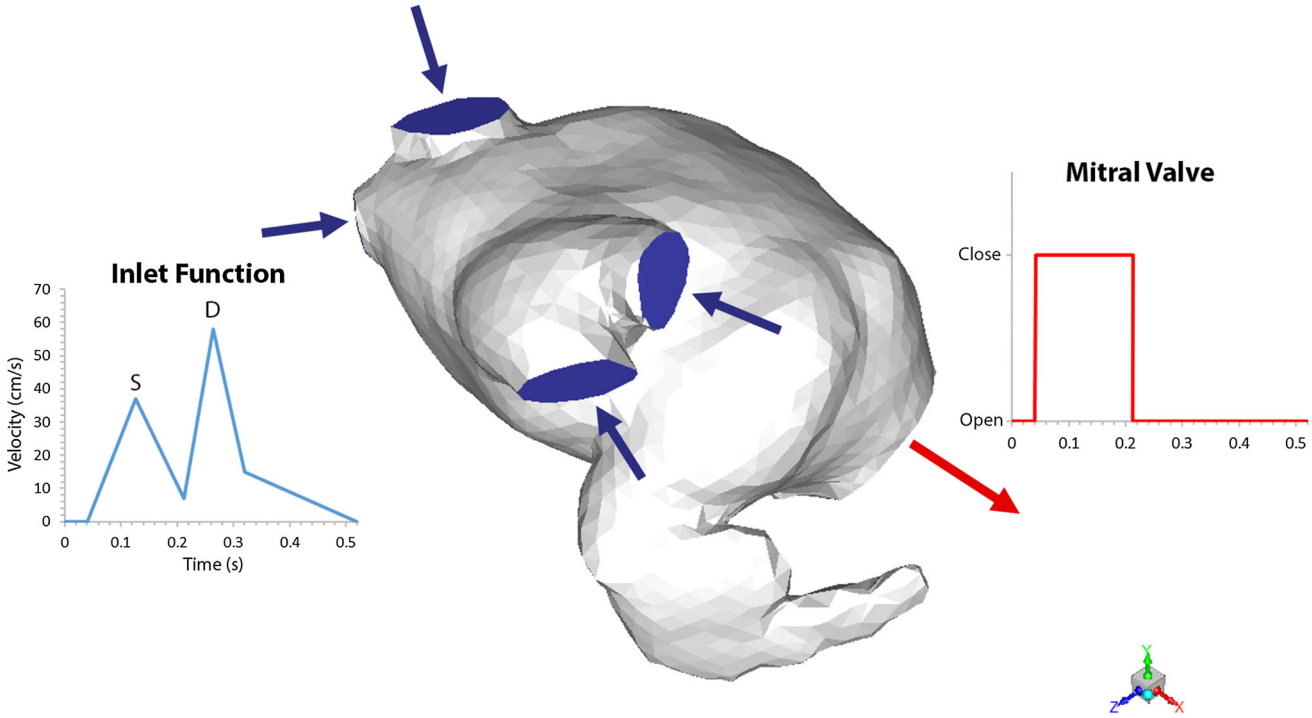


**FIGURE 8. Finite element volumetric model for left atrium with LAA. Inlet boundaries (marked in blue) and outlet boundary (marked in red), with pulmonary vein inlet flow and mitral valve outlet functions.**

the centroid of LA to the LAA ends. Since $P(I)$ is given as a stationary data (static image where the distribution remains unchanged in the Markov chain as time progresses), the normalization parameter $P(I)$ is a constant value, therefore can be neglected. The likelihood $P(I \mid A)$ for contrast HU is modeled as an approximation to a Gaussian distribution:

$$P(I \mid A) \approx \frac{1}{\sigma\sqrt{2\pi}} \exp \frac{-||\mu_c - I(p)||^2}{2\sigma_c^2} \tag{2}$$

In the process of region growing, the Gaussian parameters $\mu_c, \sigma_c$ are adaptively updated as described in Algorithm 1. The initial parameters $\mu_c = 395.8$HU, $\sigma_c = 70.3$ are estimated using intensity samples in LA regions from public CT images obtained from different patients.[45] The system updated with the parameters is

**Algorithm 1** Left Atrium Segmentation

**procedure** 3D GROW REGION($\mu_c, \sigma_c, p^*, \delta_0, l_0$)
  $V \leftarrow 0$ //visit map is all set to zero
  $\delta_{p^*} \leftarrow 0$
  enqueue $p^*$ to $Q$ //Queue
  **while** $||Q|| \neq 0$ and $\delta_{p^*} \leq \delta_0$ **do**
    $p^* \leftarrow$ dequeue an element from $Q$
    insert $p^*$ to $C$ //a point set for LA region
    **for** 26 neighbors of $p^*$ **do**
      $p \leftarrow$ one of the neighbors
      $\delta_p \leftarrow \delta_{p*} + 1$
      **if** $V(p) = 0$ and $P(A|I) \geq l_0$ **then**
        enqueue $p$ to $Q$
        update $\mu_c$ and $\sigma_c$
        $V(p) \leftarrow 1$ //visit check
      **end if**
    **end for**
  **end while**
  Return $C$
**end procedure**

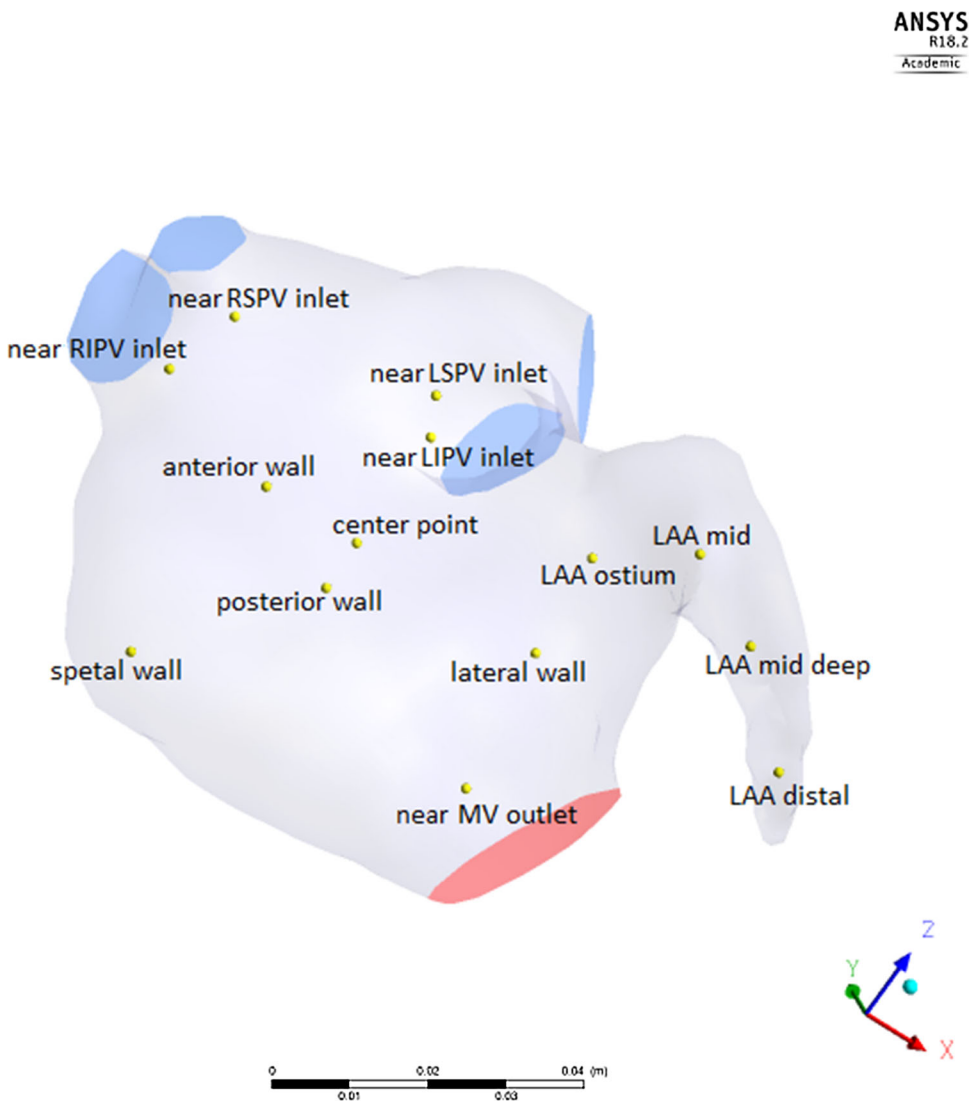


**FIGURE 9. Locations of measurement points in the LA with LAA (10 points in LA and 4 points in LAA).**

optimized for the image as the region $C$ expands gradually.

The prior $P(A)$ is modeled to penalize the distance based on the distance from the centroid of the LA to the farthest point of the LA including the LAA region. We approximate the distribution to a fall down cubic function[52] as:

$$P(A) = 2\left(\frac{\delta_p}{\delta_0}\right)^3 - 3\left(\frac{\delta_p}{\delta_0}\right)^2 + 1 \tag{3}$$

where $\delta_p$ is a geodesic distance at $p$ from the seed point. Since the LA diameter is known to be in the range of $43.1 \pm 6.4\,\text{mm}$[29], $\delta_0$ is a pre-determined distance sufficient to cover all contents including pulmonary veins (PV) and LAA. Here, $\delta_0$ is set to be 50 mm.

The fully-automated segmentation result is then compared to the ground truth (GT) result that is labeled manually. Figure 4 shows a direct comparison by overlapping the two segmented volumes on two different slices $z = 155$ and $z = 185$. Since LA is a spacious blood pool, most of the GT and the automatically segmented volumes overlap. The difference, most evidently on slice $z = 185$, is largely due to the presence or the absence of PVs. The proposed algorithm is designed to include some PV regions for simulation purpose as PV regions are important parts in the simulations. The PVs are not manually labeled in the GT results. Dice similarity coefficient (DSC) is used to quantify the similarity between the two volumes, defined as:

$$DSC(S_1, S_2) = \frac{2|S_1 \cap S_2|}{|S_1| + |S_2|} \tag{4}$$

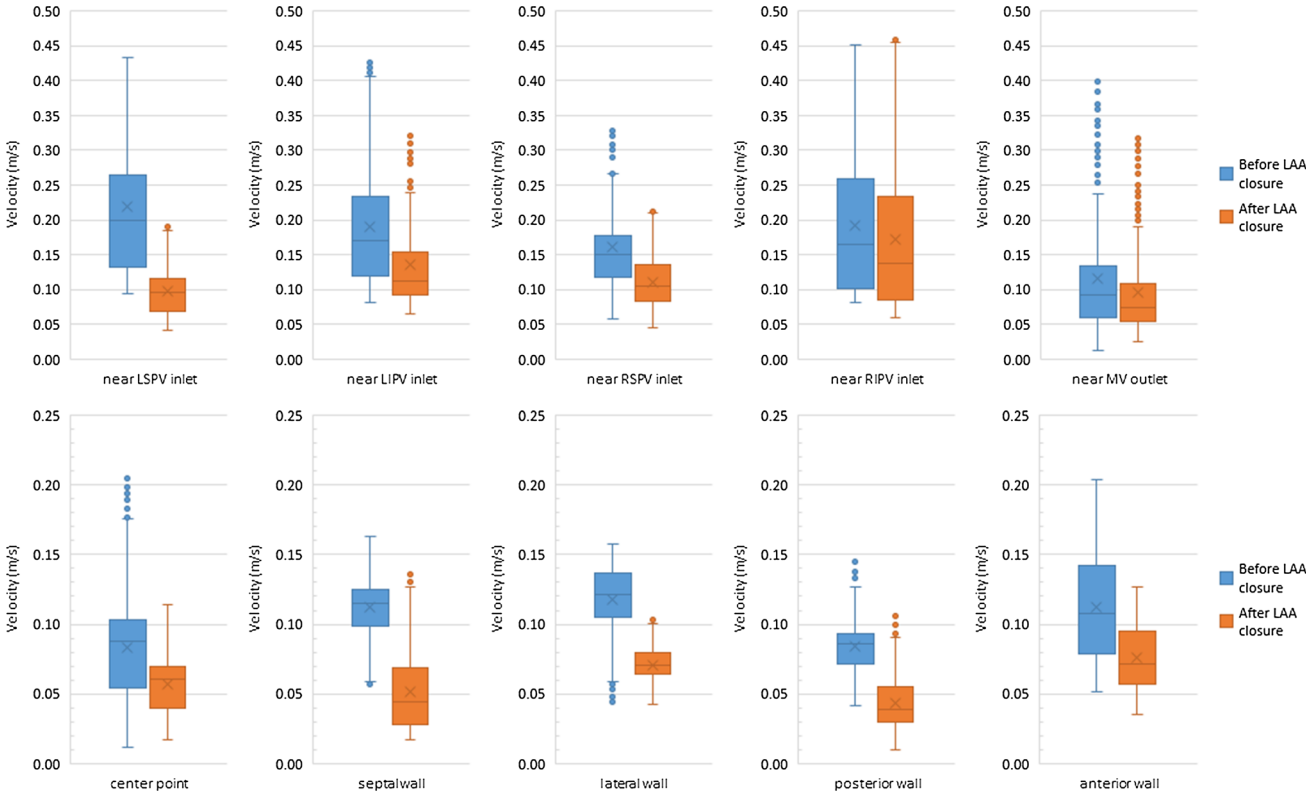


**FIGURE 10. Blood flow velocity box and whisker plots at 10 locations in LA pre- and post-LAA closure.**

To demonstrate the accuracy of the approach, we collected a total of five CT images and the corresponding GTs that are manually labeled. The average DSC measurement is found to be 86.3%. Most of the error is due to the inclusion of PV regions as mentioned previously.

The entire process takes 0.5–1 min from detecting the LA seed point to obtaining segment $C$ of the LA/LAA/PVs, to a defined geometry using vertex points. The initial segment $C$ in Algorithm 1 by now contains some small branches of the PVs since their HUs are similar to the LA. We then manually cut the branches to make the inlet and outlet planes using 3D Slicer.[25]

Once the LA with LAA geometry is completed, it is further cut to represent the geometry of post-procedure of LAA occlusion. In this case, post-procedure geometry is a simple cut of the pre-procedure geometry with LAA. This simplification can be justified and confirmed by examining the X-ray images with contrast injection. Before the procedure of LAA occlusion, LAA can be observed by contrast injection (Fig. 5(a)). After the procedure, near plane-like boundary is observed at the ostium of LAA (Fig. 5(b)). Contrast injection could not reach the LAA in the current case (Fig. 5(c)). Hence, the boundary near the occluded LAA is assumed to be near plane, and the geometry without LAA is made by cutting at the ostium of the LAA.

### *Surface and Volume Mesh Reconstruction*

The surfaces of the LA with and without LAA are reconstructed based on the vertex, or the polygon file, obtained from the image processing steps described in "Automatic LA Seed Point Detection" and LA/LAA Segmentation sections. The polygon file is imported into Meshlab[13] for surface construction and manipulation. Since the polygon file only contains vertex location information, the normal for each vertex is computed using normals for point sets function referring to 10 nearest vertices. The orientation information for the original vertex cloud is processed with default settings in Meshlab which are suitable for performing screened poisson surface reconstruction.[23] The surface meshes are further coarsened/reduced for faster 3D geometry generation. Quadric edge collapse decimation[19] is used to achieve 10,000 target elements for the geometry with LAA and 8,000 target elements for the geometry without LAA. The final surface meshes for both cases are shown in Fig. 6a. After the surface geometry is cleaned up and smoothened, the surface mesh is converted into a volume mesh that represents a fluid domain filled with blood. The surface mesh gen-

erated from the geometry is saved in Drawing Interchange Format and then imported into AUTODESK INVENTOR (Autodesk Inc., San Rafael, California, USA). The Stitch function is used to transform surface information into a solid part, as shown in Fig. 6b. Planar cuts are performed at all four pulmonary venous inlet locations normal to the blood inflow direction, assuming the blood flow direction is parallel to the vein centerlines. This step is necessary in making clearly defined inlet and outlet boundary planes that are normal to the flow directions, since a non-tangential initial velocity on the inlets would induce initial vortices. The final volumes are exported to ANSYS Fluent[2] with Initial Graphics Exchange Specification (IGES) format for meshing. Tetrahedron mesh[5] is used and the algorithm is set as patch independence to achieve relative uniform element size. Each element edge size limit is set to be between $4 \times 10^{-3}$ and $5 \times 10^{-3}$ m. The final volume mesh for the LA with LAA contains 57, 357 nodes and 39, 741 elements. The final mesh without LAA contains 44,445 nodes and 30,319 elements. Both meshes, LA with and without LAA, are shown in Fig. 6c. Various mesh sizes are also constructed for mesh convergence tests. The final meshes described here are the optimal meshes without compromising solution accuracy.

### *Simulation Setup*

Flow simulations are performed using ANSYS Fluent on both LA with and without LAA geometries. The calculations are run with a time step size of 0.0013 s and 65 iterations per time step to ensure solution convergence. Each cardiac cycle is 0.52 s. A total of 4000 time steps is run, which represents 10 cardiac cycles to ensure periodicity in the solution is achieved. The residual monitor indicates that the continuity equation is converged to $10^{-5}$ and the momentum equation is converged to $10^{-8}$ in each time step. Each run requires approximately 8 computational hours with Fluent serial processing on a AMD 1950X CPU with 16 processes of 4.0 GHz clock speed.

### *Blood Flow Modeling*

The blood in LA/LAA is modeled as Newtonian, homogeneous and incompressible fluid with a density of $\rho = 1060\,\text{kg/m}^3$ and a dynamic viscosity of $\mu = 0.0035$ kg/(ms). Bulk flow properties are sufficient assumptions for physiological blood flow in large cavities such as the atrium.[28,53] The four inlet pulmonary vein diameters range from 11.58 to 19.1 mm in this case, which yield Reynolds numbers ranging from 1,616 to 2,660 at the peak inlet velocity of 46 cm/s. These Reynolds numbers fall within the physiological range that does not require any turbulent models. The blood flow velocity $\mathbf{v}$ and pressure $p$ are solved using Navier–Stokes equations,[53] where the continuity and momentum equations are shown in Eq. (5) without considering the body force:

$$\begin{aligned} \nabla \cdot \mathbf{v} &= 0 \\ \rho(\mathbf{v}_{,t} + \mathbf{v} \cdot \nabla \mathbf{v}) &= -\nabla p + \mu \nabla^2 \mathbf{v} \end{aligned} \tag{5}$$

### *Boundary Conditions*

The simulation framework is targeted to patients with atrial fibrillation. During atrial fibrillation, the LA volume is at a dilated state with little change in volume. The LA contractility typically ranges from $26.3 \pm 10.4\%$, contrary to the LA contractility with normal sinus rhythm ($45.4 \pm 13.9\%$).[20] The LA contractility, or ejection fraction (EF, represented in %) is defined as:

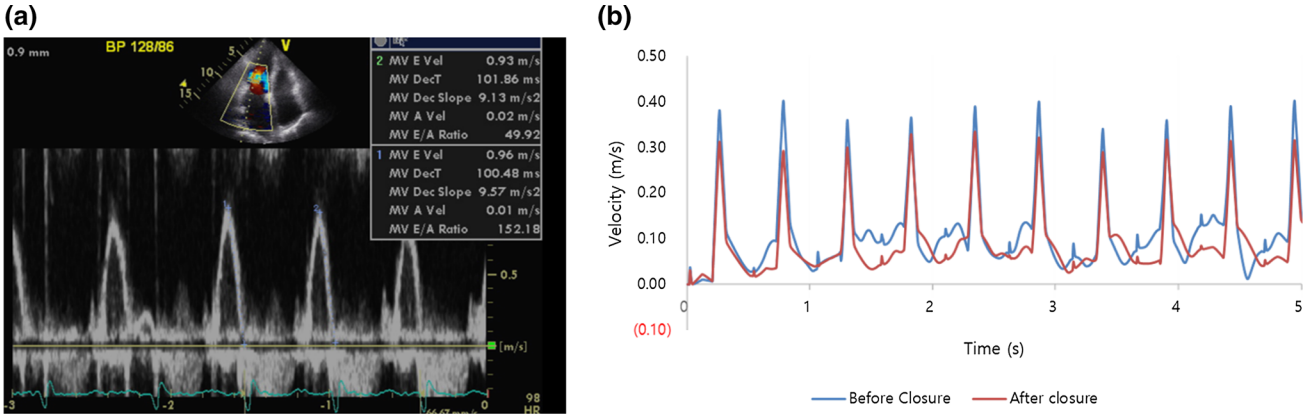


**FIGURE 11. (a) The current patient's doppler data, (b) velocities during our simulation.**

$$\text{atrial ejection fraction}\,(\%) = \frac{\text{max. volume} - \text{min. volume}}{\text{max. volume}} \quad (6)$$

The larger the EF value, the greater the contractility. We extracted LA segmentations for one cardiac cycle and the volumes are measured, shown in Fig. 7. The patient is seen to have only 13% LA contractility (min volume = 156.63 ml, max volume = 180.73 ml) due to atrial fibrillation. In this case, the LA of the current patient is at a dilated state with little change in volume. Justified by the small change in volume and to simplify the simulation process we assume the volumes of LA and LAA do not change over the cardiac cycle. Currently, this is a limitation in our capability in simulating a wider range of atrial contractilities. This is stated in "Study Limitations" section. We will include this feature in our future studies.

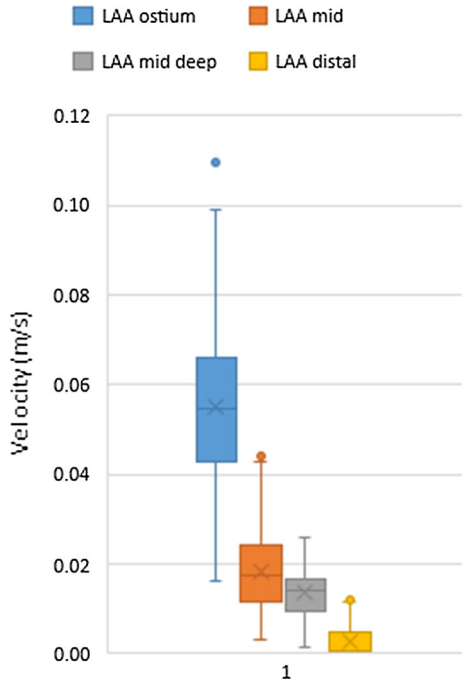


**FIGURE 12. Blood flow velocity box and whisker plot of the key points in LAA.**

When the LA is relaxed (atrial diastole), blood flows into the left atrium from the pulmonary veins. As blood flows into the atrium, the pressure rises, the blood moves passively from the atrium into the ventricle. When the action potential triggers the muscles in the atrium to contract (atrial systole), the pressure within the atrium rises further, pumping blood into the ventricles. The flow boundary conditions imposed in this study emulate atrial fibrillation where an atrial fibrillation waveform is prescribed with a forward systolic (S) phase and a diastolic (D) phase.[24,42,53] The main feature of an atrial fibrillation waveform is the missing of a proper atrial contraction phase. The waveform for one cardiac cycle is shown in Fig. 8. Since both geometries with and without LAA have the same PVs, only the geometry of LA with LAA is presented here to demonstrate the boundary condition setup. Inflow velocity is prescribed on the four pulmonary veins, labeled in Fig. 8.

The outlet of the flow is at the mitral valve. To properly simulate the opening and closing of the mitral valve, an outflow boundary condition is set to be at the closed position during the systole phase (from 40 to 212 ms) within each cardiac cycle.[36] During the remaining 348 ms in the cycle, the outlet boundary

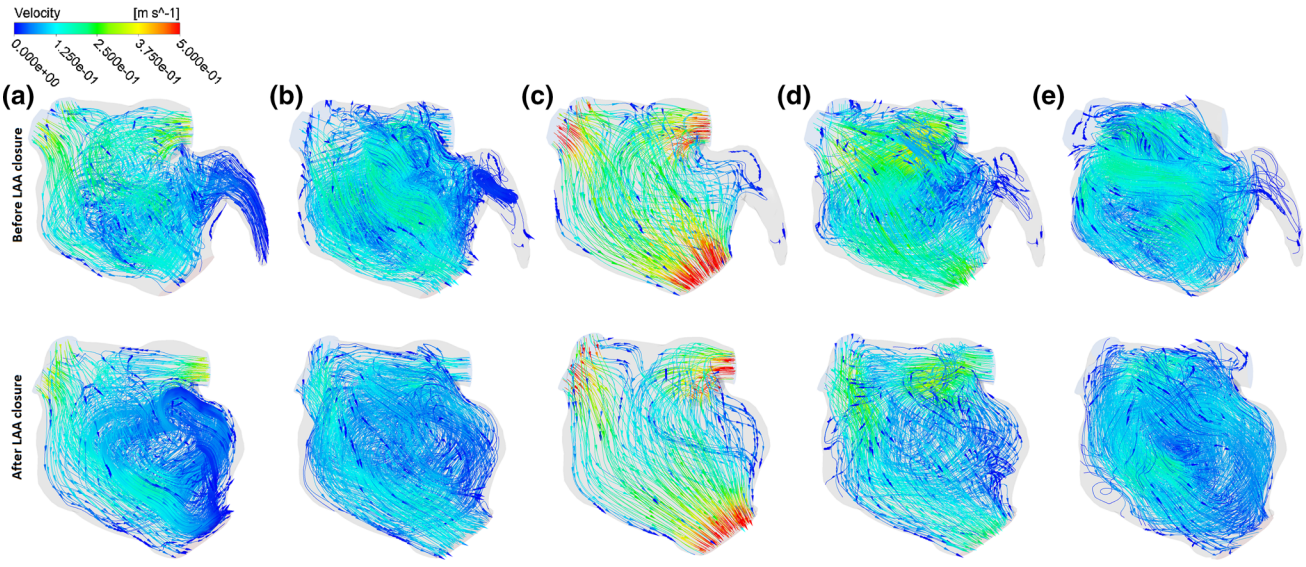


**FIGURE 13. Comparison of blood flow velocity patterns between left atrium with LAA (top) and without LAA (bottom) during (a) systole, (b) between systole and diastole, (c) diastole, (d) end diastole, and (e) end/start of cardiac cycle.**

condition is set to be 'stress-free' representing a completely opened mitral valve. The closing and opening alternation is also shown in Fig. 8. The gauge pressure at the flow exit is set to be 0 Pa. Setting such inflow and outflow conditions may result in local violation of mass balance equation (also observed in the slightly higher residual in solving the continuity equation, $10^{-5}$ vs. $10^{-8}$ for the momentum equation). But it overall does not severely impact the solution as some relaxations are allowed in the solving process.

## RESULTS

In this section, the detailed hemodynamics flow characteristics are closely examined for the cases of LA with and without LAA, representing the flows pre- and post-LAA closure. These flow characteristics, i.e. velocities, streamline, and vortices, are known to affect thrombus formation.

### *Flow Velocities*

To compare blood flow velocities, ten location points are chosen in the LA for both geometries pre- and post-LAA closure (labeled in Fig. 9). Figure 10 compares the velocity magnitudes for the two cases at

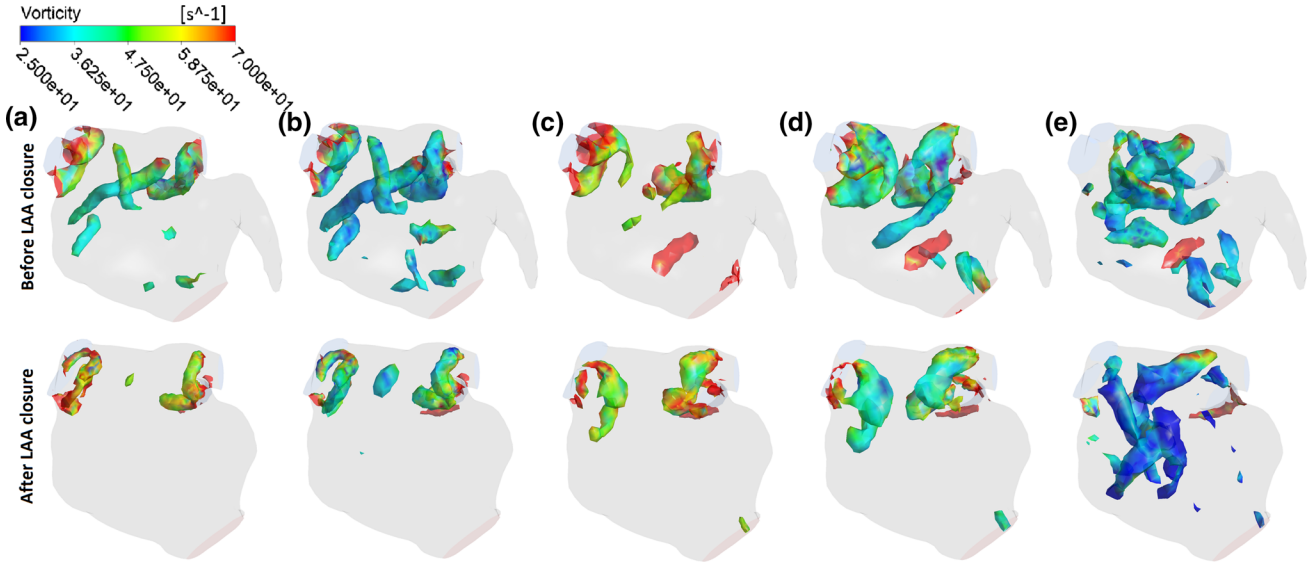


**FIGURE 14. Left atrium peak vortices region with vorticity colored: (a) early systole, (b) peak systole, (c) early diastole, (d) peak diastole, and (e) end cardiac cycle.**

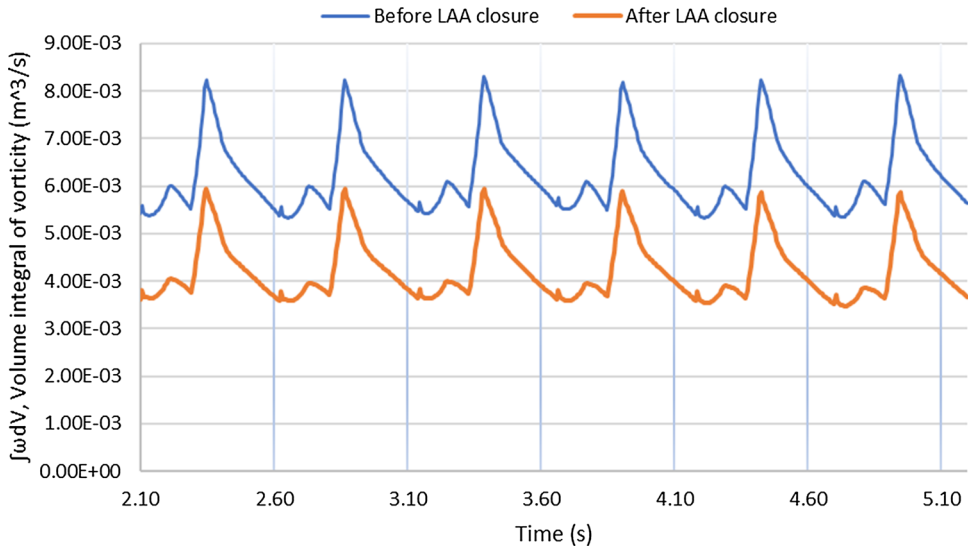


**FIGURE 15. The volume integral of vorticity over the fluid domain for the 5th to 10th cardiac cycles during the CFD simulation.**

these 10 locations using box and whisker plots. Generally, average velocity magnitudes are significantly reduced in post-LAA closure (median velocity: 8.61 cm/s, interquartile range (IQR): 5.92 to 11.07) compared to pre-LAA closure (median velocity: 11.66 cm/s, IQR: 11.02 to 19.07) with $P = 0.002$ by Wilcoxon test. The median difference of the average velocity between pre- and post-LAA closure is −4.05 cm/s (95% confidence interval −7.02 to −2.80, by Hodges–Lehmann test). Except for the left superior pulmonary vein inlet velocity (54% decrement), velocity magnitudes in most pulmonary vein inlets and mitral valve outlet portions show slight changes (10 to 30% decrement). However, in septal (51%), posterior (41%), and lateral wall (41%), the velocity magnitudes are significantly reduced after LAA closure.

To validate the simulation result, we further compared the velocity near MV (exit) to the doppler data of the patient, shown in Fig. 11. We found they have very similar magnitudes and patterns, notably the LA contractile phase is missing in the wave form resulting from an atrial fibrillation.

Four additional location points are chosen in the LAA (also labeled in Fig. 9): LAA ostium, LAA mid, LAA mid deep, and LAA distal, to evaluate the velocity magnitudes inside LAA. The LAA ostium plane is defined as the plane where LAA orifice intersects with the LA. The mass flow rate through the LAA ostium plane is measured and found to be 0.02 kg/s. Velocity magnitudes in LAA are significantly reduced as the flow goes deeper inside LAA beginning at 5.78 cm/s in the ostium and ending at 0.29 cm/s in the distal portion of LAA (shown in the box and whisker plot in Fig. 12). Most significant to note is that the velocity at distal LAA ranges from 0.04 to 1.31 cm/s, implying that the flow is almost stagnant.

### *Flow Streamlines and Vortices in the LA: Comparison Between Pre and Post-LAA Closure*

The blood flow is also depicted using streamlines (Fig. 13) at five distinct instances: (a) systole, (b) between systole and diastole, (c) diastole, (d) end diastole, and (e) end/start of a cardiac cycle. The snapshots are taken during the fourth cardiac cycle in the simulation when the flow has reached a periodic solution over each cardiac cycle. The streamlines show more disorganized and turbulent patterns in the pre-LAA closure case than in the post-LAA closure case. This is evident upon an observation that a more direct path towards the mitral valve outlet is found upon LAA closure.

To illustrate the flow patterns more clearly in 3D views, vortices are presented in Fig. 14. Vortex strength and duration are often the key indications of future thrombolic events.[48] Vortex core locations are plotted in both pre- and post-LAA closure cases. Five snapshots are taken at (a) early systole, (b) peak systole, (c) early diastole, (d) peak diastole, and (e) end cardiac cycle. The locations are identified by Q-criterion at where the value Q is greater than 0.35. During systole, the maximum diameter of the vortex core region is smaller in the post-LAA closure model (1.0 cm) than in the pre-LAA closure model (1.7 cm). During diastole, peak vortex diameters are also reduced from 2.8 cm pre-LAA closure to 1.5 cm post-LAA closure. Furthermore, there are clear reductions in the number and strength of vortices scattered in the LA. They can be visually identified by the color contours by comparing all phases throughout the cardiac cycle.

In the pre-LAA closure model, the first set of vortices appears during the early systole phase between 110 and 175 ms lasting around 65 ms. The strength and spread of the vortices peak at 135 ms (Fig. 14b). The second set of vortices in the pre-LAA closure model is developed during mid-diastole and decreased during late-diastole, from 210 to 420 ms. It results in a 210 ms duration and peaking around 245 ms (Fig. 14d). On the other hand, in the post-LAA closure model, the first set of vortices occurs between 130 and 170 ms continuing for approximately 40 ms, which is significantly shorter than the pre-LAA closure model. The spread and strength of the first set of vortices peak at 155 ms (Fig. 14b). The second set of vortices in the post-LAA closure model occurs between 230 ms and 365 ms during diastole, lasting for 135 ms which is also significantly shorter than in the pre-LAA closure model. The peak vortices occur at 265 ms (Fig. 14d). Overall, the vortex duration is dramatically decreased from 65/210 ms pre-LAA closure to 40/135 ms post-LAA closure based on modeling, which is a significant reduction as a result of the LAA closure.

The total reduction of vorticity strength can be quantified by the volume integral of the vorticity over the LA domain. Figure 15 shows the volume integral of the vorticity over the last six cardiac cycles (5th–10th) during the simulation, which clearly demonstrates the periodic pattern and a significant reduction (25%) in the vorticity magnitude, from a peak of $8 \times 10^{-3}$ to $6 \times 10^{-3} m^3/s$.

## DISCUSSION

In this study, we aim to establish a predictive framework for patient-specific CFD simulations of percutaneous LAA closure procedures by comparing pre- and post-LAA closure states. The framework includes automatic segmentation of patient-specific CT

images of LA with LAA, and CFD hemodynamic analysis.

To achieve a fully-automated segmentation process, we propose a novel LA detection and segmentation algorithm. The concept of using geometric relations in cardiac CT to achieve full automation was first introduced by one of the authors.[21] The method estimates multiple objects simultaneously considering their anatomical geometrical relations. To our knowledge, it was the first of its kind ever introduced in the field. In this work, we improve and expand this method to find the centroid (a seed) of the left atrium (LA). The position of the LA can be detected automatically without any user interactions. In addition, region growing method is also much improved in this study. Region growing is one of the general segmentation methods. We modify and optimize the algorithm for LA segmentation by adopting Bayesian estimation with distance as the prior. We assume that the likelihood follows Gaussian distribution, and the expectation in Eq. (2) is dynamically updated, which optimizes itself during the growing process. As a result, our fully automated segmentation approach (0.5 to 1 min) is significantly faster than semi-automatic segmentation (5 to 10 min) available using commercial software.

Upon image segmentation, a finite element model is built including proper application of flow boundary conditions at the four pulmonary veins and mitral valve. Dynamic CFD analysis is performed in both pre- and post-LAA closure models. The CFD simulation results are presented as velocity magnitudes and patterns, visual flow patterns using streamlines, and vortices which are considered closely related to thrombus formation. We demonstrate that flow velocity magnitudes are significantly reduced. The hemodynamics inside LAA are also investigated. In the distal portion of the LAA, the velocity magnitudes decrease to nearly 0 cm/s during the entire diastolic phase, indicating flow stagnation inside the deep pocket formed in LAA. In this condition, it is highly probable that thrombi accumulate deep inside LAA.[32,39,47,50] The flow streamlines are greatly stabilized, and mitral outlet patterns appear to be more organized after LAA closure. More significantly, we find that vortices are dramatically reduced in their size, strength, number, and duration upon LAA occlusion.

A previous study presented the blood flow simulations inside LA with appendage by using the fluid-structure interaction finite element method, but the study was performed using an idealized geometrical model.[31] Since a geometric model was not obtained from a real patient, the simulated results had limitations and, as a result, clinically meaningful conclusions for specific patients could not be drawn. A more recent study showed the CFD simulation framework for the left heart system including left atrium, left ventricle, and aorta based on an actual patient's CT scan. They presented the flow rates, vorticity magnitudes, and velocity vector scales of the left heart obtained from 4D CT images using the temporal interpolation technique and non-linear image registration algorithm.[12] The study was geared toward the left ventricle and therefore meant that a detailed evaluation of LA and LAA was not performed.[16] To our knowledge, our study is the first to present a simulation framework evaluating the clinical impact of LAA and the efficacy of the LAA closure in each individual based on CT images.

## STUDY LIMITATIONS

Our study has several limitations. In this study, we used one patient-specific LA/LAA case for the validation of our proposed framework. To make the framework as a clinically-useful diagnostic and predictive tool, more validation studies with patient data are necessary.

Fixed LA and LAA volumes are assumed in this study as the patient under study has atrial fibrillation with a LA contractility of only 13%. In reality, atrial fibrillation patients have fibrillatory LA and LAAs that are pathologically enlarged in concurrent with severely decreased contractility. Thus, representing the precise irregular and rapid movement (of up to 300 beats/min) for the LA/LAA during a cardiac cycle is challenging.[30] Inevitably, a fixed boundary assumption had to be used in this study. The assumption of a non-dilated LA is in fact a limitation in our study at this point. We are currently working on developing capabilities to handle moving and deformable boundaries using 4D patient-specific CT data so that a large range of contractilities can be represented in the simulation framework.

In this particular patient-specific study, the inlet and outlet blood flow boundary conditions are imposed with as an approximation rather than from directly extracted from patient-specific data. In the follow-up studies, patient-specific boundary conditions will be incorporated for more accurate predictions of LAA occlusion procedures.

The simulation studies currently do not include the prediction of quantities such as wall shear stress, particle residence time, wall shear oscillatory index, *etc*. These parameters provide more direct measurements on thrombus formation risks of future thrombotic events. Further post-processing of primitive variables will be included in future studies.

## CONCLUSIONS

In this study, we demonstrated a clinically-relevant CFD simulation study of the effect of LAA closure using imaged-based LA and LAA. The framework involved first obtaining a patient specific CT image of LA and LAA, which was then processed in an automated manner to setup for CFD analysis. Upon imaging segmentation, a finite element model was built including properly applying flow boundary conditions at the four pulmonary veins and mitral valve. In this study, we specifically examined flow characteristics, e.g. velocity, flow patterns, and vortices in two cases, LA with and without LAA, to mimic LAA closure procedure. Comparison between the results showed that LAA closure had significant impact on blood flow velocity and paths. LAA closure also successfully reduced left atrial vortices in strength and duration which indicated that LAA closure surgery was effective in reducing flow patterns that were associated to thrombus formation. This study provides an efficient and effective way of analyzing and comparing hemodynamic parameters on patient-specific LA and LAA, which can be further utilized for candidate selection process and procedure planning.

Future framework will include building a moving finite element mesh based on 4D CT scans that simulates the expansion and contraction of the LA and LAA volumes. The corresponding CFD analysis will be based on a moving mesh. Further patient data will be acquired such as the patient-specific pulmonary inflow measurement and a more accurate representation of the mitral valve outflow boundary condition. A thorough result investigation can also benefit from an extensive flow analysis related to flow structure characterization of vortex properties as the ones shown in Refs. [11,14,26,43], and [46].

## ELECTRONIC SUPPLEMENTARY MATERIAL

The online version of this article (https://doi.org/10.1007/s13239-019-00412-7) contains supplementary material, which is available to authorized users.

## FUNDING

Author LTZ would like to acknowledge the support from NSFC Grants 11650410650 and 11550110185. Authors BJ, HP and HC are supported by Leading Foreign Research Institute Recruitment Program through the National Research Foundation of Korea (NRF) funded by the Ministry of Science, ICT & Future Planning (MSIP) (2012027176).

## CONFLICT OF INTEREST

All authors declare that they have no conflicts of interest.

## ETHICAL APPROVAL

No human or animal studies were carried out by the authors for this article. The institutional review board approved this study and waived the requirement for informed consent due to its retrospective design.

## REFERENCES

[1]3D-Doctor Brochure. Abel software Corp. 2019.
[2]ANSYS, Inc. ANSYS Academic Research, Release 18, Fluent, 2017.
[3]Adams, R. and L. Bischof. Seeded region growing. *IEEE Trans. Pattern Anal. Mach. Intell.* 16(6):641–647, 1994.
[4]Al-Saady, N. M., O. A. Obel, and A. J. Camm. Left atrial appendage: structure, function, and role in thromboembolism. *Heart* 82(5):547–554, 1999.
[5]Alliez, P., D. Cohen-Steiner, M. Yvinec, and M. Desbrun. Variational tetrahedral meshing. *ACM Trans. Graph.* 24(3):617–625, July 2005.
[6]Backer, O. D., S. Arnous, N. Ihlemann, N. Vejlstrup, E. Jørgensen, S. Pehrson, T. D. W. Krieger, P. Meier, L. Søndergaard, and O. W. Franzen. Percutaneous left atrial appendage occlusion for stroke prevention in atrial fibrillation: an update. *Open Heart* 1(1):e000020, 2014.
[7]Bansal, M. and R. R Kasliwal. Echocardiography for left atrial appendage structure and function. *Indian Heart J.* 64(5):469–475, 2012.
[8]Biase, L. D., J. D. Burkhardt, P. Mohanty, J. Sanchez, S. Mohanty, R. Horton, G. J. Gallinghouse, S. M. Bailey, J. D. Zagrodzky, P. Santangeli, S. Hao, R. Hongo, S. Beheiry, S. Themistoclakis, A. Bonso, A. Rossillo, A. Corrado, A. Raviele, A. Al-Ahmad, P. Wang, J. E. Cummings, R. A. Schweikert, G. Pelargonio, A. D. Russo, M. Casella, P. Santarelli, W. R. Lewis, and A. Natale. Left atrial appendage. *Circulation* 122(2):109–118, 2010.
[9]Blackshear, J. L. and J. A. Odell. Appendage obliteration to reduce stroke in cardiac surgical patients with atrial fibrillation. *Ann. Thorac. Surg.* 61(2):755–759, 1996.
[10]Bosi, G. M., A. Cook, R. Rai, L. J. Menezes, S. Schievano, R. Torii, and G. B. Burriesci. Computational fluid dynamic analysis of the left atrial appendage to predict thrombosis risk. *Front. Cardiovasc. Med.* 5:34, 2018.
[11]Caracciolo, G., H. Abe, J. Narula, P. P. Sengupta, G. Pedrizzetti, A. Kheradvar, and B. K. Khandheria. Contrast echocardiography for assessing left ventricular vortex strength in heart failure: a prospective cohort study. *Eur. Heart J.* 14(11):1049–1060, 04 2013.
[12]Chnafa, C., S. Mendez, and F. Nicoud. Image-based large-eddy simulation in a realistic left heart. *Comput. Fluids* 94:173–187, 2014.
[13]Cignoni, P., M. Callieri, M. Corsini, M. Dellepiane, F. Ganovelli, and G. Ranzuglia. Meshlab: an open-source

mesh processing tool. In: Eurographics Italian Chapter Conference, 2008, pp. 129–136.
[14]Cimino, S., G. Pedrizzetti, G. Tonti, E. Canali, V. Petronilli, L. De Luca, C. Iacoboni, and L. Agati. In vivo analysis of intraventricular fluid dynamics in healthy hearts. *Eur. J. Mech.* 35:40–46, 2012.
[15]Ernst, G., C. Stöllberger, F. Abzieher, W. Veit-Dirscherl, E. Bonner, B. Bibus, B. Schneider, and J. Slany. Morphology of the left atrial appendage. *Anat. Rec.* 242(4):553–561, 1995.
[16]Fyrenius, A., L. Wigström, T. Ebbers, M. Karlsson, J. Engvall, and A. F. Bolger. Three dimensional flow in the human left atrium. *Heart* 86(4):448–455, 2001.
[17]García-Fernández, M. A., E. G. Torrecilla, D. S. Román, J. Azevedo, H. Bueno, M. M. Moreno, and J. L. Delcán. Left atrial appendage doppler flow patterns: implications on thrombus formation. *Am. Heart J.* 124(4):955–961, 1992.
[18]García-Isla, G., A. L. Olivares, E. Silva, M. Nuñez-Garcia, C. Butakoff, D. Sanchez-Quintana, H. G. Morales, X. Freixa, J. Noailly, T. De Potter, et al. Sensitivity analysis of geometrical parameters to study haemodynamics and thrombus formation in the left atrial appendage. *Int. J. Numer. Methods Biomed. Eng.* 34(8):e3100, 2018.
[19]Hoppe, H. New quadric metric for simplifiying meshes with appearance attributes. In: Proceedings of the Conference on Visualization'99: Celebrating Ten Years, 1999, pp. 59–66.
[20]Hwang, S. H., S. Y. Roh, J. Shim, J. Choi, Y.-H. Kim, and Y.-W. Oh. Atrial fibrillation: relationship between left atrial pressure and left atrial appendage emptying determined with velocity-encoded cardiac MR imaging. *Radiology* 284(2):381–389, 2017.
[21]Jeon, B., Y. Hong, D. Han, Y. Jang, S. Jung, Y. Hong, S. Ha, H. Shim, and H.-J. Chang. Maximum a posteriori estimation method for aorta localization and coronary seed identification. *Pattern Recogn.* 68:222–232, 2017.
[22]Kanderian, A. S., A. M. Gillinov, G. B. Pettersson, E. Blackstone, and A. L. Klein. Success of surgical left atrial appendage closure. *J. Am. Coll. Cardiol.* 52(11):924–929, 2008.
[23]Kazhdan, M., and H. Hoppe. Screened poisson surface reconstruction. *ACM Trans. Graph.* 32(3):29, 2013.
[24]Keren, G., J. Sherez, R. Megidish, B. Levitt, and S. Laniado. Pulmonary venous flow pattern-its relationship to cardiac dynamics. A pulsed doppler echocardiographic study. *Circulation* 71(6):1105–1112, 1985.
[25]Kikinis, R., S. D. Pieper, and K. G. Vosburgh. 3d slicer: a platform for subject-specific image analysis, visualization, and clinical support. In: Intraoperative Imaging and Image-Guided Therapy. Berlin: Springer, pp. 277–289, 2014.
[26]Kim, I.-C., G.-R. Hong, G. Pedrizzetti, C. Y. Shim, S.-M. Kang, and N. Chung. Usefulness of left ventricular vortex flow analysis for predicting clinical outcomes in patients with chronic heart failure: a quantitative vorticity imaging study using contrast echocardiography. *Ultrasound Med. Biol.* 44(9):1951–1959, 2018.
[27]Korhonen, M., A. Muuronen, O. Arponen, P. Mustonen, M. Hedman, P. Jäkälä, R. Vanninen, and M. Taina. Left atrial appendage morphology in patients with suspected cardiogenic stroke without known atrial fibrillation. *PLoS ONE* 10(3):e0118822, 2015.
[28]Kovács, T., P. Cattin, H. Alkadhi, S. Wildermuth, and G. Székely. Automatic segmentation of the vessel lumen from 3d cta images of aortic dissection. In: Bildverarbeitung für die Medizin. Berlin: Springer, 2006, pp. 161–165.
[29]Laukkanen, J. A., S. Kurl, J. Eränen, M. Huttunen, and J. T. Salonen. Left atrium size and the risk of cardiovascular death in middle-aged men. *Arch. Intern. Med.* 165(15):1788–1793, 2005.
[30]Long, B., J. Robertson, A. Koyfman, K. Maliel, and J. R. Warix. Emergency medicine considerations in atrial fibrillation. *Am. J. Emerg. Med.* 36(6):1070–1078, 2018.
[31]Malchano, Z. J., P. Neuzil, R. C. Cury, G. Holmvang, J. Wwichet, E. J. Schmidt, J. N. Ruskin, and V. Y. Reddy. Integration of cardiac CT/MR imaging with three-dimensional electroanatomical mapping to guide catheter manipulation in the left atrium: implications for catheter ablation of atrial fibrillation. *J. Cardiovasc. Electrophysiol.* 17(11):1221–1229, 2006.
[32]Masci, A., M. Alessandrini, L. Dede, D. Forti, F. Menghini, C. Tomasi, A. Quarteroni, C. Corsi, and Ecole Polytecnique Fédérale de Lausanne EPFL CMCS. Development of a computational fluid dynamics model of the left atrium in atrial fibrillation on a patient specific basis. *Computing* 44:1, 2017.
[33]Masci, A., D. Forti, M. Alessandrini, F. Menghini, L. Dede, C. Corsi, A. Quarteroni, and C. Tomasi. Development of a patient-specific computational fluid dynamics model of the LA in AF for stroke risk assessment. *EP Europace* 19(3):120–121, 2017.
[34]Mimics. Materialise Inc. 2019.
[35]Mittal, R., J. H. Seo, V. Vedula, Y. J. Choi, H. Liu, H. H. Huang, S. Jain, L. Younes, T. Abraham, and R. T. George. Computational modeling of cardiac hemodynamics: current status and future outlook. *J. Comput. Phys.* 305:1065–1082, 2016.
[36]Nishimura, R. A., M. .D Abel, L. K. Hatle, and A. J. Tajik. Relation of pulmonary vein to mitral flow velocities by transesophageal doppler echocardiography. Effect of different loading conditions. *Circulation* 81(5):1488–1497, 1990.
[37]Ostermayer, S. H., M. Reisman, P. H. Kramer, R. V. Matthews, W. A. Gray, P. C. Block, H. Omran, A. L. Bartorelli, P. D. Bella, C. Di Mario, C. Pappone, P. N. Casale, J. W. Moses, A. Poppas, D. O. Williams, B. Meier, A. Skanes, P. S. Teirstein, M. D. Lesh, T. Nakai, Y. Bayard, K. Billinger, T. Trepels, U. Krumsdorf, and H. Sievert. Percutaneous left atrial appendage transcatheter occlusion (plaato system) to prevent stroke in high-risk patients with non-rheumatic atrial fibrillation. *J. Am. Coll. Cardiol.* 46(1):9–14, 2005.
[38]Otani, T., A. Al-Issa, A. Pourmorteza, E.R. McVeigh, S. Wada, and H. Ashikaga. A computational framework for personalized blood flow analysis in the human left atrium. *Ann. Biomed. Eng.* 44(11):3284–3294, 2016.
[39]Pollick, C. and D. Taylor. Assessment of left atrial appendage function by transesophageal echocardiography. Implications for the development of thrombus. *Circulation* 84(1):223–231, 1991.
[40]Pozzoli, M., O. Febo, A. Torbicki, R. Tramarin, G. Calsamiglia, F. Cobelli, G. Specchia, and J. R. T. C. Roelandt. Left atrial appendage dysfunction: a cause of thrombosis? Evidence by transesophageal echocardiography-doppler studies. *J. Am. Soc. Echocardiogr.* 4(5):435–441, 1991.
[41]Price, M. J. V. Y. Reddy, M. Valderrábano, J. L. Halperin, D. N. Gibson, N. Gordon, K. C. Huber, and D. R. Holmes. Bleeding outcomes after left atrial appendage closure compared with long-term warfarin: a pooled, pa-

tient-level analysis of the watchman randomized trial experience. *JACC Cardiovasc. Interv.* 8(15):1925–1932, 2015.

[42]Rajagopalan, B., C. D. Bertram, T. Stallard, and G. de J. Lee. Blood flow in pulmonary veins: III simultaneous measurements of their dimensions, intravascular pressure and flow. *Cardiovasc. Res.* 13(12):684–692, 1979.

[43]Sampath, K., T. T. Harfi, R. T. George, and J. Katz. Optimized time-resolved echo particle image velocimetry–particle tracking velocimetry measurements elucidate blood flow in patients with left ventricular thrombus. *J. Biomech. Eng.* 140(4):041010, 2018.

[44]Saygi, S., U. O. Turk, E. Alioglu, B. Kirilmaz, I. Tengiz, N. Tuzun, and E. Ercan. Left atrial appendage function in mitral stenosis: is it determined by cardiac rhythm? *J. Heart Valve Dis.* 20(4):417–424, 2011.

[45]Schaap, M., C. T. Metz, T. van Walsum, A. G van der Giessen, A. C. Weustink, N. R. Mollet, C. Bauer, H. Bogunović, C. Castro, X. Deng, et al. Standardized evaluation methodology and reference database for evaluating coronary artery centerline extraction algorithms. *Med. Image Anal.* 13(5):701–714, 2009.

[46]Sengupta, P. P., G. Pedrizzetti, P. J. Kilner, A. Kheradvar, T. Ebbers, G. Tonti, A. G. Fraser, and J. Narula. Emerging trends in cv flow visualization. *JACC Cardiovasc. Imaging* 5(3):305–316, 2012.

[47]Shrestha, N. K., F. L. Moreno, F. V. Narciso, L. Torres, and H. B. Calleja. Two-dimensional echocardiographic diagnosis of left-atrial thrombus in rheumatic heart disease. a clinicopathologic study. *Circulation* 67(2):341–347, 1983.

[48]Smith, R. L., E. F. Blick, J. Coalson, and P. D. Stein. Thrombus production by turbulence. *J. Appl. Physiol.* 32(2):261–264, 1972.

[49]Tabata, T., T. Oki, A. Iuchi, H. Yamada, K. Manabe, K. Fukuda, M. Abe, N. Fukuda, and S. Ito. Evaluation of left atrial appendage function by measurement of changes in flow velocity patterns after electrical cardioversion in patients with isolated atrial fibrillation. *Am. J. Cardiol.* 79(5):615–620, 1997.

[50]Vigna C., A. Russo, V. De Rito, G. Perna, A. Villella, M. Testa, V. Sollazzo, R. Fanelli, and F. Loperfido. Frequency of left atrial thrombi by transesophageal echocardiography in idiopathic and in ischemic dilated cardiomyopathy. *Am. J. Cardiol.* 70(18):1500–1501, 1992.

[51]Wang, Y. A. N., L. D. Biase, R.P. Horton, T. Nguyen, P. Morhanty, and A. Natale. Left atrial appendage studied by computed tomography to help planning for appendage closure device placement. *J. Cardiovasc. Electrophysiol.* 21(9):973–982, 2010.

[52]Wyvill, G., C. McPheeters, and B. Wyvill. Data structure forsoft objects. *Vis. Comput.* 2(4):227–234, 1986.

[53]Zhang, L. T. and M. Gay. Characterizing left atrial appendage functions in sinus rhythm and atrial fibrillation using computational models. *J. Biomech.* 41(11):2515–2523, 2008.